Characteristics of laser operation at 1064 nm in Nd:YVO4 under diode pumping at 808 and 914 nm

Xavier Délen, François Balembois, Patrick Georges

Characteristics of laser operation at 1064 nm in Nd:YVO_4 under diode pumping at 808 and 914 nm

Xavier Délen,[1,*] François Balembois,[1] Olivier Musset,[2] and Patrick Georges[1]

[1]*Laboratoire Charles Fabry de l'Institut d'Optique, CNRS, Université Paris-Sud, Campus Polytechnique, RD 128, 91127 Palaiseau Cedex, France*
[2]*Laboratoire Interdisciplinaire Carnot de Bourgogne, UMR 5209 CNRS-Université de Bourgogne, 9 Avenue A. Savary, BP 47 870, F-21078 Dijon Cedex, France*
**Corresponding author: xavier.delen@institutoptique.fr*

Received July 12, 2010; revised October 22, 2010; accepted October 25, 2010; posted October 27, 2010 (Doc. ID 131551); published December 10, 2010

A comparative study between 808 and 914 nm pumping of Nd:YVO_4 crystals for laser operation at 1064 nm has been carried out. Using similar setups, performances of both configurations were first studied in the continuous wave, small-signal gain, and Q-switched regimes. Thanks to a numerical model, it is shown that fluorescence quenching and upconversion processes limit the possible uses for the 914 nm pumping scheme to regimes with low population inversions. © 2010 Optical Society of America

OCIS codes: 140.3530, 140.3540, 140.6810, 140.3613.

1. INTRODUCTION

Nd:YVO_4 is a widely used laser material that has led to the demonstration of many laser systems in the past two decades [1–3]. First pumped at 808 nm because it corresponds to the maximum of absorption, Nd:YVO_4 can also be pumped at other wavelengths. Lowering the quantum defect by pumping at 888 or 880 nm allows one to reduce the thermal load and to increase the optical efficiency [4,5]. Sangla *et al.* demonstrated almost 80% efficiency in a CW regime using direct in-band pumping at 914 nm [6]. In-band pumping implies the use of highly doped and long crystals to compensate for the lower absorption cross sections. For example, a 1.5% doped Nd:YVO_4 crystal has been used for 914 nm pumping, whereas 0.1% to 0.5% doped crystals are generally used for 808, 880, and 888 nm pumping. This concentration difference may induce parasitic effects, as new sources of heat load have been observed using high doping concentration in Nd:YVO_4 [7–9]. In this paper, we propose to carry out a comparison between 808 and 914 nm pumping with a similar setup for laser operation at 1064 nm. Section 2 compares the two pumping configurations in the CW regime. In Section 3, small-signal gain measurements are presented and compared with theoretical values obtained with a numerical simulation. In Section 4, we compare the two pumping solutions for Q-switched operation and discuss the configuration in which the use of 914 nm pumping can be interesting. Finally, we compare the thermal power generated by 808, 888, and 914 nm pumping in order to find the appropriate laser regimes for the two pumping configurations.

2. CW OPERATION

The experimental setup is described in Fig. 1. We used two fiber-coupled laser diodes (one at 808 nm and one at 914 nm) with the same output characteristics ($\Phi = 100\,\mu$m; NA = 0.22; $P_{out} = 35$ W). The laser cavity consisted of three mirrors: M_1, M_2, and M_3. M_1 is a plane dichroïc mirror with high transmission at the pump wavelength (99% at 808 nm and 98.4% at 914 nm) and high reflectivity at 1064 nm. The concave mirror M_2 is highly reflective at the laser wavelength and partly transparent at the pump wavelengths. Its radius of curvature is −100 mm. The plane output coupler is M_3 and has a transmission of 15% at 1064 nm. The cavity was designed with a length $M_1M_2 = 200$ mm and $M_2M_3 = 56$ mm, such that the beam radius reached about 250 μm in the Nd:YVO_4. To match the laser beam, the output of the pump fiber was imaged with a single doublet with a magnification of 5. Thanks to their large radii (250 μm), the pump beam size and the cavity beam size can be considered as constant in the Nd:YVO_4. Consequently, the overlap between the two beams is excellent. This simplifies the modeling carried out in this work.

Because of the very large difference of absorption between 808 and 914 nm, we chose two Nd:YVO_4 crystals with completely different concentrations: 1.5% doped crystal for 914 nm pumping and 0.1% for 808 nm pumping. The crystals have the same geometry (section 3 × 3 mm^2; length 10 mm) with M_1 directly coated on the input face. Despite the strong difference in doping concentration, the absorptions are not the same: 44% for 914 nm pumping and 75% for 808 nm pumping. Consequently, the comparison between the two pumping configurations will be carried out for the same absorbed pump power. As the beams have a constant size in the gain media, the pumping conditions are relatively similar for a same absorbed pump power. As the absorbed pump power changes under laser operation, it was controlled measuring the pump power transmitted through the M_2 mirror.

Figure 2 shows the results in CW operation. A slope efficiency of 81% was obtained for 914 nm pumping and a 58% slope efficiency for 808 nm pumping. In CW operation, the difference of quantum defect results in a difference of

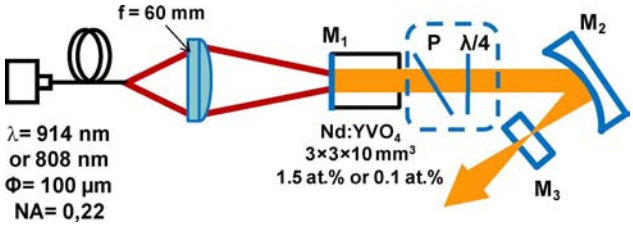

Fig. 1. (Color online) Experimental setup used for CW experiments. M_1 is coated on the crystal (HT808/HT914/HR1064). M_2 is a $R = -100$ mm concave mirror and M_3 is the plane output coupler ($T = 15\%$). The insert contains elements used for gain measurement: P stands for polarizer and $\lambda/4$ stands for quarter wave plate.

slope efficiency and the 914 nm pumping is advantageous. Not only is the efficiency higher, but the lower thermal load also induces a reduced thermal lens and potentially allows much higher pump power before crystal fracture.

In this experiment, the slope efficiency ratio between the two pumping wavelengths is not equal to the quantum efficiency ratio. Indeed, the efficiency at 808 nm is slightly lower than expected. This can be explained by two factors: the output coupler used was the optimum for 914 nm and not for 808 nm pumping. Moreover, the losses might be slightly higher in the 808 nm configuration. However, the advantage of 914 nm pumping over 808 nm pumping is obvious since the slope efficiency obtained with 914 nm pumping is six percentage points above the theoretical quantum defect limited slope efficiency with 808 nm pumping (75%).

During CW operation with relatively high-reflectivity output couplers ($R = 85\%$), the gain is highly saturated and the inversion of population density is kept low. The impact of nonradiative effects appearing at high doping concentration is then minor. This is not necessarily the case in Q-switched or amplification regimes, which generally require higher population inversion. The basic quantity ruling those regimes is the small-signal gain. Its evolution versus absorbed pump power is measured in Section 3 for 808 and 914 nm pumping.

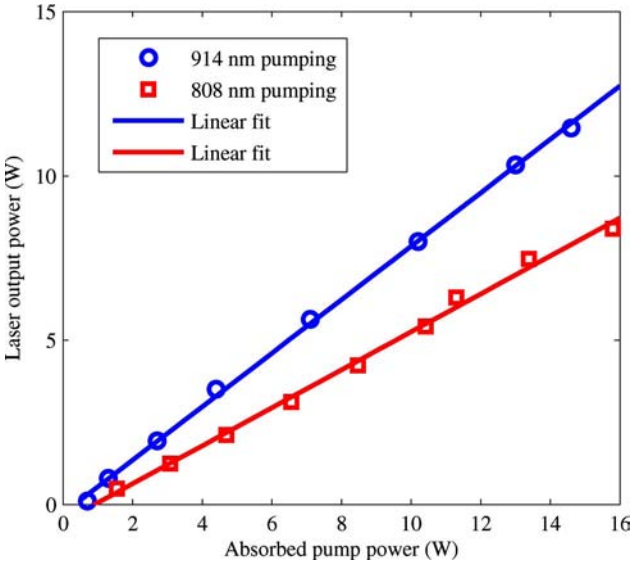

Fig. 2. (Color online) Efficiency curves for 914 nm pumping (circles) and 808 nm pumping (squares). Linear fitting (solid curves) gives 81% slope efficiency for 914 nm and 58% slope efficiency for 808 nm pumping.

3. SMALL-SIGNAL GAIN MEASUREMENTS

To measure the small-signal gain, the method described by Balembois *et al.* [10] was used. The knowledge of the cavity losses gives the value of the small-signal gain at the threshold. By changing the losses, the small-signal gain versus the pump power can be recorded. A polarizer and a quarter wave plate were used to introduce variable losses in the cavity (see insert in Fig. 1). At the threshold, the overall reflectivity of the cavity over a round trip R and the double pass small-signal gain G_0^2 are linked by Eq. (1):

$$G_0^2 R = 1. \tag{1}$$

The exponential form of the expression of G_0^2 is given in Section 4.A (see Eq. (6)).

Figure 3 shows double pass small-signal gain denoted G_0^2 measurements for increasing absorbed pump power. A significant difference of behavior appears between the two pumping solutions. The small-signal gain curve as a function of the absorbed pump power has an exponential-like shape for the 808 nm pumping, whereas the evolution is almost linear for the 914 nm pumping. The maximal small-signal gain value obtained for about 11 W of absorbed pump power at 808 nm was more than 55, whereas it was about five times lower for the same absorbed pump power at 914 nm. In contrast with what has been observed in CW regime, the 914 nm pumping solution shows poor performance in terms of small-signal gain. This performance might be explained by the use of a high doping concentration of Nd:YVO_4 (1.5%), which enhances a large increase of nonradiative effects. In order to understand this behavior, Section 4 is devoted to a modeling of small-signal gain.

4. MODELING

In this section, the modeling for 808 nm pumping in order to obtain theoretical values of the small-signal gain is first carried out, followed by a description of the more complicated modeling for a pumping at 914 nm.

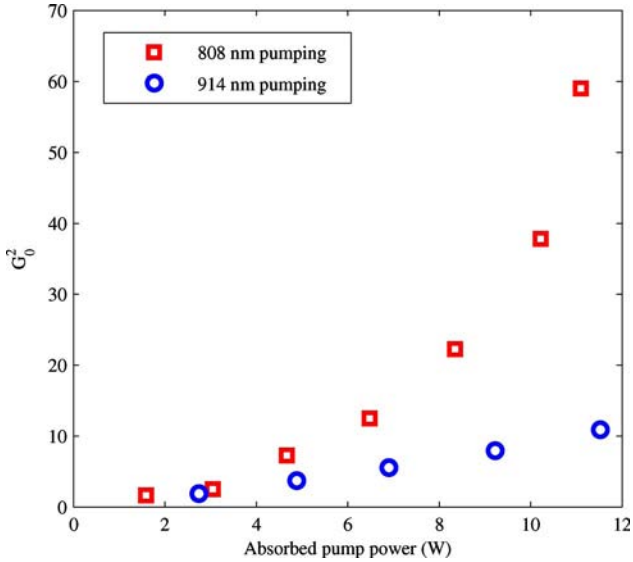

Fig. 3. (Color online) Experimental double pass small-signal gain at 1064 nm versus absorbed pump power for 914 nm pumping (circles) and 808 nm pumping (squares).

A. Modeling for 808 nm Pumping

A top-hat distribution can describe approximately the beam profile of a fiber-coupled diode [8,11,12]. As both pump and signal beams have large Rayleigh lengths compared to the crystal longitudinal dimension, both beam radii will be considered as constant along the crystal. As the problem also presents an axial symmetry, only z dependence will be considered. Equation (2) is the usual rate equation for four level systems considering different absorption cross sections for the two polarizations as it is the case for Nd:YVO_4 pumped at 808 nm:

$$\frac{d\Delta n}{dt} = (\sigma_a^{pc} I_p^c + \sigma_a^{pa} I_p^a)(n_t - \Delta n) - \frac{\Delta n}{\tau}, \tag{2}$$

where τ is the upper state lifetime (measured value of $\tau = 98\,\mu$s for 0.1% doping concentration) [13], σ_a^{pa} and σ_a^{pc} are the absorption cross sections at the pump wavelengths for each polarization ($\sigma_a^{pa} = 0.79 \times 10^{-19}$ cm^2 and $\sigma_a^{pc} = 3.2 \times 10^{-19}$ cm^2) [14], I_p^a and I_p^c are the pump intensities for each polarization, Δn is the population inversion density, and n_t is the total population density. The local stationary solution of Eq. (2) is given by

$$\Delta n(z) = n_t \tau \frac{\sigma_a^{pc} I_p^c(z) + \sigma_a^{pa} I_p^a(z)}{1 + \frac{I_p^c(z)}{I_{\text{psat}}^c} + \frac{I_p^a(z)}{I_{\text{psat}}^a}}, \tag{3}$$

where $I_{\text{psat}}^a = 1/(\sigma_a^{pa}\tau)$ and $I_{\text{psat}}^c = 1/(\sigma_a^{pc}\tau)$ are the pump saturation intensities for each polarization. Taking pump absorption saturation into account and assuming the lower level of the laser transition is not to be populated, the absorption coefficient $\alpha_p(z)$ is given by

$$\alpha_p(z) = \sigma_a^p n_t - \sigma_a^p \Delta n(z). \tag{4}$$

For the calculation, the crystal is cut in elementary slices of length dz, where dz is small enough to obtain a result independent of its value. Pump intensity, population inversion, and absorption coefficients are found in each slice using Eqs. (3) and (4), the knowledge of $I_p(0)$, and Eq. (5), which gives the pump intensity in the slice $z + dz$:

$$I_p(z + dz) = I_p(z) \exp(-\alpha(z) dz). \tag{5}$$

The overall double pass small-signal gain G_0^2 at 1064 nm can be deduced by numerical integration using

$$G_0^2 = \exp\left(2 \int_0^L \sigma_e^l \Delta n(z) \mathrm{d}z\right), \tag{6}$$

where σ_e^l is the emission cross section at 1064 nm ($\sigma_e^l = 12 \times 10^{-19}$ cm^2) [15,16]. As shown by Fig. 4, theoretical gain values fit the set of experimental data for a pumping at 808 nm. A slight adjustment of the pump waist radius to 287 μm was done in order to obtain this fit. The adjusted value of the beam radius, close to the experimental one, is used as a reference in Subsection 4.B.

B. Modeling for 914 nm Pumping

The model is then applied for a pumping at 914 nm. As the absorption of the pump is independent of polarization at 914 nm, the two polarizations are not distinguished. As stimulated emission at the pumping wavelength can occur for 914 nm pumping, Eq. (7) is used to calculate $\Delta n(z)$:

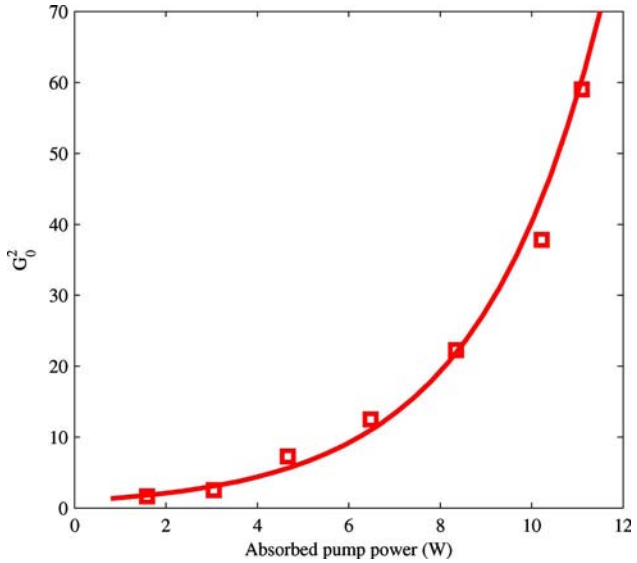

Fig. 4. (Color online) Theoretical (solid curve) and experimental (squares) double pass small-signal gain at 1064 nm versus absorbed pump power.

$$\frac{d\Delta n}{dt} = \sigma_a^p I_p n_t - (\sigma_a^p + \sigma_e^p) I_p \Delta n - \frac{\Delta n}{\tau}, \tag{7}$$

where σ_e^p is the emission cross section at the pump wavelength ($\sigma_e^p = 0.48 \times 10^{-19}$ cm^2) [17] and σ_a^p is the absorption cross section at the pump wavelength ($\sigma_a^p = 0.04 \times 10^{-19}$ cm^2 at 914 nm) [6]. Unique local stationary solution of Eq. (7) is given by

$$\Delta n(z) = n_t \tau \frac{\sigma_a^p I_p(z)}{1 + \frac{I_p(z)}{I_{\text{psat}}}}, \tag{8}$$

where $I_{\text{psat}} = 1/(\sigma_a^p + \sigma_e^p)\tau$ is the pump saturation intensity. Figure 5 shows the results obtained by numerical simulation and experimental data (see curve 1 in Fig. 5). The model described above clearly appears to fail. While the calculation gives an expected gain of more than 130, the experimental value is near 11 for 11.7 W of absorbed pump power.

In the case of highly doped crystals, parasitic effects limiting the population inversion need to be considered: the two main effects are the fluorescence quenching and the upconversion process. Fluorescence lifetime is reduced at high doping concentrations due to concentration-dependent fluorescence quenching. The combination of migration of excitation and excitation trapping with cross relaxation is responsible for this effect and also results in higher heat generation [13]. Defining a nonradiative decay time τ_{nr} enables one to take this effect into account using rate equations. The fluorescence lifetime τ is then given by

$$\frac{1}{\tau} = \frac{1}{\tau_{sp}} + \frac{1}{\tau_{nr}}. \tag{9}$$

The fluorescence lifetime for our two samples has been measured to be 98 and 68 μs for 0.1% and 1.5% doped samples, respectively.

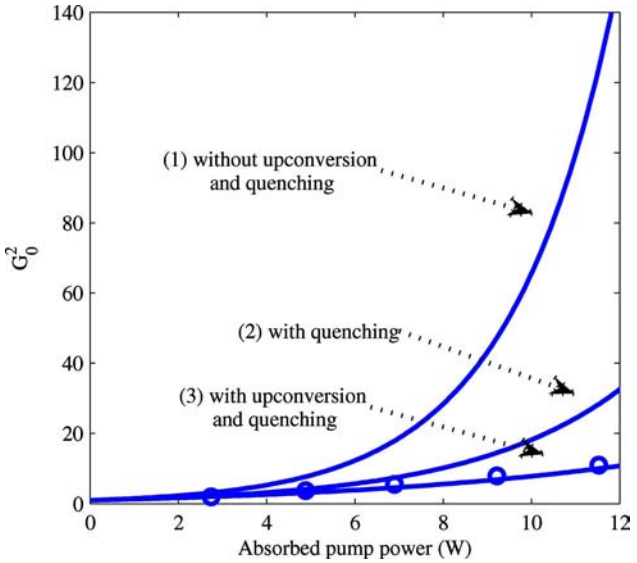

Fig. 5. (Color online) Theoretical double pass small-signal gain at 1064 nm versus absorbed pump power at 914 nm (solid curves) and experimental double pass small-signal gain (circles) under different hypotheses. Pump waist radius: $w_p = 287\,\mu$m.

Even if an accurate description of upconversion is difficult to obtain, the $-\gamma\Delta n^2$ term where γ is the upconversion rate is widely used to evaluate the role of this process in the excited level depopulation [9,18,19]. The rate equation for the population inversion can be written as

$$\frac{d\Delta n}{dt} = \sigma_a^p I_p n_t - (\sigma_a^p + \sigma_e^p) I_p \Delta n - \frac{\Delta n}{\tau_{nr}} - \frac{\Delta n}{\tau_{sp}} - \gamma \Delta n^2. \quad (10)$$

Unique local stationary solution is given by

$$\Delta n(z) = \frac{1}{2\gamma}\left(-\left((\sigma_a^p + \sigma_e^p) I_p(z) + \frac{1}{\tau}\right) + \left\{\left[(\sigma_a^p + \sigma_e^p) I_p(z) + \frac{1}{\tau}\right]^2 + 4\gamma\sigma_a^p I_p(z) n_t\right\}^{1/2}\right). \quad (11)$$

γ can be measured by performing fluorescence decay measurement. Chen *et al.* measured $\gamma = 1.5 \pm 0.5 \times 10^{-21}\,\mathrm{m}^3/\mathrm{s}$ for a 0.5% doped Nd:YVO_4 and Meilhac *et al.* measured $\gamma = 3 \pm 1 \times 10^{-21}\,\mathrm{m}^3/\mathrm{s}$ for a 1% doped Nd:YVO_4 [18,20]. If we assume that the upconversion rate increases quadratically with the concentration, as indicated in the literature [19], we can expect a value of $\gamma = 10 \pm 4 \times 10^{-21}\,\mathrm{m}^3/\mathrm{s}$ for 1.5% doped Nd:YVO_4, knowing the experimental results for other concentrations.

Curve 3 in Fig. 5 shows the fit obtained using the model accounting for fluorescence quenching and upconversion, close to experimental data. An upconversion rate parameter of $7 \times 10^{-21}\,\mathrm{m}^3/\mathrm{s}$ has been used to fit the experimental data (see curve 3 in Fig. 5). This value is within the uncertainty range of the one calculated using literature data. This is the only fit parameter, all other parameters come from the simulations for 808 nm pumping and the literature. The calculated G_0^2, when taking into account only the fluorescence quenching, is still about three times higher than measured values for 11.7 W of absorbed pump power (see curve 2 in Fig. 5). This shows that both effects have a significant influence on small-signal gain for the configuration considered in this paper.

As shown in this section, nonradiative effects reduce the small-signal gain dramatically. Section 5 shows how these parasitic effects can strongly affect a laser regime dependent on population inversion, such as the Q-switched regime.

5. Q-SWITCHED OPERATION

Using a rubidium titanyle phosphate electro-optical modulator inserted between M1 and M2, we tested our cavities in the Q-switched regime. The experimental setup is shown on Fig. 6. An optimal coupler $T = 20\%$ was found in both cases. Table 1 summarizes a few significant results for two repetition rates: 10 and 20 kHz.

In all cases, the pulse durations were similar: approximately 30 ns. Despite higher values of absorbed pump power at 914 nm, the laser average output power at 1064 nm was still lower than what has been obtained with 808 nm pumping. This result is in agreement with the small-signal gain studies presented earlier: the nonradiative effects limit the population inversion at 914 nm and, consequently, the performance in the Q-switched regime.

The difference of performance between the two pumping configurations is more pronounced at 10 kHz than at 20 kHz. Indeed, more population inversion can be stored in the gain medium at 10 kHz. It leads to an increase of the number of nonradiative desexcitations affecting the performance for the 914 nm pumping.

The efficiency reduction due to nonradiative effects is coupled with a thermal load increase, which should also be considered as it might induce beam distortion and ultimately crystal fracture. This is the purpose of Section 6.

6. HEAT GENERATION VERSUS PUMPING WAVELENGTH

The goal of this section is to compare theoretically the heat loads in Nd:YVO_4 crystals usually used for laser action. Similar analysis applied to Nd:YAG can be found in other papers [21,22]. 808 nm pumping and 914 nm pumping will be considered. We added calculations for 888 nm pumping to complete the study, as this pumping gives very interesting results [4,23–25]. Upconversion and fluorescence quenching are nonradiative effects that are intrinsically related to additional sources of heating, and the heat loads can, therefore, be higher than the one brought by the quantum defect (defined by $\eta_Q = (\nu_p - \nu_l)/\nu_l$, where ν_p is the the pump frequency and ν_l is the laser frequency). Using the rate equation model, we can compute the fractional thermal loading denoted as η_H and corresponding to the ratio of the power dissipated by nonradiative (i.e., thermal) effects to the absorbed pump power.

Table 1. Experimental Results in Q-Switched Regime for Optimal Coupling Value T = 20% and Absorbed Pump Power of 13.5 W for 914 nm Pumping and 11.4 W for 808 nm Pumping[a]

	10 kHz	20 kHz
808 nm	$P = 2.7$ W $\eta = 23\%$	$P = 3.2$ W $\eta = 28\%$
914 nm	$P = 2.1$ W $\eta = 16\%$	$P = 2.9$ W $\eta = 21\%$

[a] P is the average output power and η the optical efficiency.

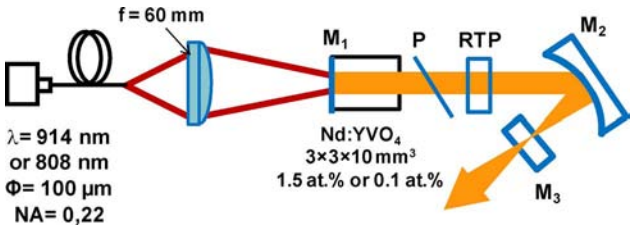

Fig. 6. (Color online) Experimental setup used for Q-switched regime.

It is a key parameter since it is related to the temperature increase inside the crystal and even to the maximum pump power the crystal can stand before fracture.

For the sake of simplicity, this ratio is considered in a small volume of gain medium, such that the population inversion density Δn and the pumping rate R (meaning the number of ions excited from the ground state to the upper state per second and per unit volume) are supposed to be constant. η_H can be expressed by Eq. (12) if we suppose that the pump quantum efficiency is equal to unity (meaning that one absorbed photon leads to one atom in the excited state) and if we consider only an emission at 1064 nm, corresponding to the main transition in Nd:YVO_4:

$$\eta_H = \eta_Q + \frac{\nu_l}{R\nu_p}\left(\frac{\Delta n}{\tau_{nr}} + \gamma \Delta n^2\right). \tag{12}$$

Under steady-state and continuous pumping, the maximal population inversion density that can be reached Δn_0 can be calculated by solving the rate equations given in Section 4:

$$\Delta n_0 = \frac{-\frac{1}{\tau} + \left(\frac{1}{\tau^2} + 4\gamma R\right)^{1/2}}{2\gamma}. \tag{13}$$

For the computation we choose a 0.1% Nd for a pumping at 808 nm, a 1.5% Nd at 914 nm, and 0.5% Nd at 888 nm (the last one is in accordance with [4]). For the sake of comparison, we consider an identical pumping rate R for all cases even if it might correspond to different incident pump power (due to different absorption coefficients). To be coherent with the previous sections, the pumping rate chosen corresponds to the maximal value theoretically obtained with a top-hat profile 35 W 914 nm pump beam focused on a diameter of 600 μm in an a-cut 1.5% doped Nd:YVO_4 crystal ($R = 1.7 \times 10^{29}$ ph.m^{-3}.s^{-1}). In the three cases, we calculate η_H by taking into account the pump wavelength and the two parameters that are concentration-dependent (τ_{NR} and γ). The results are presented in Fig. 7.

The points A, B, and C represent the fractional thermal loading and maximal population inversion under steady-state and continuous pumping for the three cases. The population inversions are strongly different, being much higher under 808 nm pumping (point A) than 914 nm pumping (point C). In accordance with the previous sections, this means that the small-signal gain is much higher under 808 nm pumping. Conversely, the heat generation is much higher under 914 nm pumping, reaching almost 80% of the pump power, very far from the quantum defect.

We also investigated the variation η_H versus Δn, the pumping rate remaining constant. Indeed, the saturation of Δn might be very different depending on the laser regime (CW

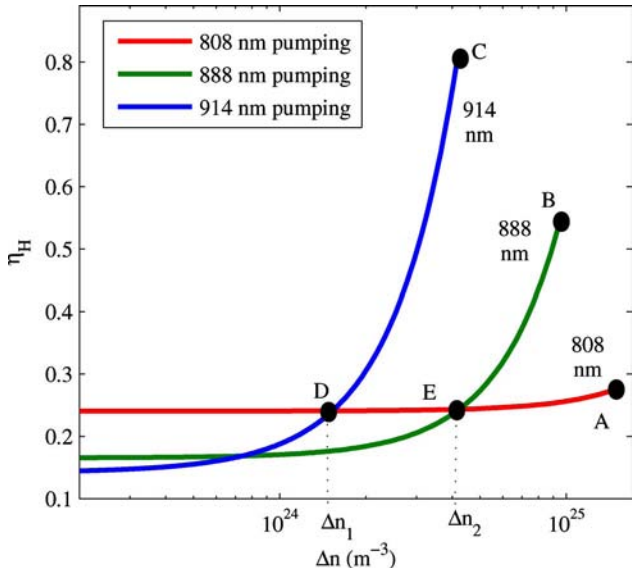

Fig. 7. (Color online) Fractional thermal loading versus inversion of population density for a fixed pumping rate ($R = 1.7 \times 10^{29}$ ph.m^{-3}.s^{-1}) and three pumping wavelengths and doping concentrations (808 nm/0.1%, 888 nm/0.5%, and 914 nm/1.5%).

oscillators with different output coupling, Q-switch oscillators, or amplifiers). In all pumping configurations, a decrease of population inversion leads to a limitation of the parasitic effects and to a reduction of the thermal load. The thermal ratio tends toward the quantum defect [as can be seen in Eq. (12)] when the population inversion density tends toward zero. As expected, it becomes lower under 914 nm than under 808 nm pumping. However, to reach this ideal configuration, the population inversion needs to be strongly saturated, with a value below Δn_1 (see point D in Fig. 7). This can occur only in laser oscillators having low losses or in high repetition rate power amplifiers.

Pumping at 888 nm seems to be an interesting intermediate. The population inversion can reach much higher values than under 914 nm pumping (point B), and the range of population inversion limiting the heat generation below the one at 808 nm is extended compared to a pumping at 914 nm (see point E and Δn_2). However, the fractional thermal loading can reach values that are much higher than the quantum defect. This means that laser operation with pumping at 888 nm must be considered carefully in order to reduce the thermal effects.

7. CONCLUSION

The excellent results obtained in CW were promising and clearly demonstrated advantages for the 914 nm pumping solution. In contrast, further investigations developed in this paper show better performance for the 808 nm pumping solution in terms of small-signal gain and Q-switched operation. Upconversion processes and nonradiative decays were identified as the phenomena responsible for this difference.

Considering the heat generated in the gain medium and the population inversion density, our work tends to identify the laser regimes where 914 nm pumping is advantageous. In the case of the CW regime in a low-loss cavity or in the case of high repetition rate power amplifiers, the population inversion can be strongly limited by laser saturation and the heat generation tends toward the quantum defect. This has two consequences on the laser operation: the laser is very efficient

and the thermal load is strongly limited. In these regimes, power scaling at larger values than under 808 nm pumping is possible.

For laser regimes requiring high gain value (i.e., high population inversion density), for example, in Q-switched regime or for preamplifiers, the use of 808 nm pumping is clearly more advantageous in terms of gain and thermal load. The basic advantage of this pumping wavelength is the strong absorption, allowing the use of very low doped crystals, which limits the nonradiative effects. In between, pumping at 888 nm appears to be an interesting intermediate that needs to be considered carefully for high gain laser regimes.

To extend the operation range of the 914 nm pumping, one can think of using lower doping concentrations. This needs to be compensated by an increase of the interaction length between the medium and the pump beam: multipass pumping geometry (such as the thin disk concept) or crystal fibers may be considered for this purpose.

REFERENCES

1. R. A. Fields, M. Birnbaum, and C. L. Fincher, "Highly efficient Nd:YVO_4 diode-laser end-pumped laser," Appl. Phys. Lett. **51**, 1885–1886 (1987).
2. P. C. Shardlow and M. J. Damzen, "20 W single longitudinal mode Nd:YVO_4 retro-reflection ring laser operated as a self-intersecting master oscillator power amplifier," Appl. Phys. B **97**, 257–262 (2009).
3. V. Z. Kolev, M. J. Lederer, B. Luther-Davies, and A. V. Rode, "Passive mode locking of a Nd:YVO_4 laser with an extra-long optical resonator," Opt. Lett. **28**, 1275–1277 (2003).
4. L. McDonagh, R. Wallenstein, R. Knappe, and A. Nebel, "High-efficiency 60 W TEM_{00} Nd:YVO_4 oscillator pumped at 888 nm," Opt. Lett. **31**, 3297–3299 (2006).
5. Y. Sato, T. Taira, N. Pavel, and V. Lupei, "Laser operation with near quantum-defect slope efficiency in Nd:YVO_4 under direct pumping into the emitting level," Appl. Phys. Lett. **82**, 844–846 (2003).
6. D. Sangla, M. Castaing, F. Balembois, and P. Georges, "Highly efficient Nd : YVO_4 laser by direct inband diode pumping at 914 nm," Opt. Lett. **34**, 2159–2161 (2009).
7. A. Sennaroglu, "Influence of neodymium concentration on the strength of thermal effects in continuous-wave diode-pumped Nd:YVO_4 laser at 1064 nm," Opt. Quantum Electron. **32**, 1307–1317 (2000).
8. Y. F. Chen, Y. P. Lan, and S. C. Wang, "Modeling of diode-end-pumped Q-switched solid-state lasers: influence of energy-transfer upconversion," J. Opt. Soc. Am. B **19**, 1558–1563 (2002).
9. V. Ostroumov, T. Jensen, J. P. Meyn, G. Huber, and M. A. Noginov, "Study of luminescence concentration quenching and energy transfer upconversion in $LaSc_3(BO_3)_4$ and $GdVO_4$ laser crystals," J. Opt. Soc. Am. B **15**, 1052–1060 (1998).
10. F. Balembois, F. Falcoz, F. Kerboull, F. Druon, P. Georges, and A. Brun, "Theoretical and experimental investigations of small-signal gain for a diode-pumped Q-switched Cr:LiSAF laser," IEEE J. Quantum Electron. **33**, 269–278 (1997).
11. Y. F. Chen, T. M. Huang, C. F. Kao, C. L. Wang, and S. C. Wang, "Optimization in scaling fiber-coupled laser-diode end-pumped lasers to higher power: influence of thermal effect," IEEE J. Quantum Electron. **33**, 1424–1429 (1997).
12. Y. F. Chen, "Design criteria for concentration optimization in scaling diode end-pumped lasers to sigh powers: influence of thermal fracture," IEEE J. Quantum Electron. **35**, 234–239 (1999).
13. Z. Huang, Y. Huang, Y. Chen, and Z. Luo, "Theoretical study on the laser performances of Nd^{3+}:YAG and Nd^{3+}:YVO_4 under in-direct and direct pumping," J. Opt. Soc. Am. B **22**, 2564–2569 (2005).
14. W. Koechner, *Solid-State Laser Engineering* (Springer, 1999).
15. A. W. Tucker, M. Birnbaum, C. L. Fincher, and J. W. Erler, "Stimulated-emission cross section at 1064 and 1342 nm in Nd:YVO_4," J. Appl. Phys. **48**, 4907–4911 (1977).
16. R. D. Peterson, H. P. Jenssen, and A. Cassanho, "Investigation of the spectroscopic properties of Nd:YVO_4," in *Advanced Solid-State Lasers*, M. E. Fermann and L. R. Marshall, eds., Trends in Optics and Photonics Series (Optical Society of America, 2002), Vol. 68, paper TuB17.
17. C. Czeranowsky, M. Schmidt, E. Heumann, G. Huber, S. Kutovoi, and Y. Zavartsev, "Continuous wave diode pumped intracavity doubled Nd:$GdVO_4$ laser with 840 mw output power at 456 nm," Opt. Commun. **205**, 361–365 (2002).
18. L. Meilhac, G. Pauliat, and G. Roosen, "Determination of the energy diffusion and the Auger upconversion constants in a Nd:YVO_4 standing wave laser," Opt. Commun. **203**, 341–347 (2002).
19. S. Guy, C. L. Bonner, D. P. Shepherd, D. C. Hanna, and A. C. Tropper, "High-inversion densities in Nd:YAG: upconversion and bleaching," IEEE J. Quantum Electron. **34**, 900–909 (1998).
20. Y. F. Chen, C. C. Liao, Y. P. Lan, and S. C. Wang, "Determination of the Auger upconversion rate in fiber-coupled diode end-pumped Nd:YAG and Nd:YVO_4 crystals," Appl. Phys. B **70**, 487–490 (2000).
21. D. C. Brown, "Heat, fluorescence, and stimulated-emission power densities and fractions in Nd:YAG," IEEE J. Quantum Electron. **34**, 560–572 (1998).
22. N. Pavel, V. Lupei, J. Saikawa, T. Taira, and H. Kan, "Neodymium concentration dependence of 0.94-, 1.06- and 1.34 μm laser emission and of heating effects under 809- and 885 nm diode laser pumping of Nd:YAG," Appl. Phys. B **82**, 599–605 (2006).
23. L. McDonagh and R. Wallenstein, "Low-noise 62 W CW intracavity-doubled TEM_{00} Nd:YVO_4 green laser pumped at 888 nm," Opt. Lett. **32**, 802–804 (2007).
24. L. McDonagh, R. Wallenstein, and A. Nebel, "111 W, 110 MHz repetition-rate, passively mode-locked TEM_{00} Nd:YVO_4 master oscillator power amplifier pumped at 888 nm," Opt. Lett. **32**, 1259–1261 (2007).
25. M. C. Nadeau, S. Petit, P. Balcou, R. Czarny, S. Montant, and C. Simon-Boisson, "Picosecond pulses of variable duration from a high-power passively mode-locked Nd:YVO_4 laser free of spatial hole burning," Opt. Lett. **35**, 1644–1646 (2010).